Gradus Vol 11, No 3 (2024)
ISSN 2064-8014

# PARAMETRIC STUDY OF COAXIAL DEEP BOREHOLE HEAT EXCHANGERS TO DETERMINE PEAK PERFORMANCE AND ZONE OF INFLUENCE

*József Pap*[0000-0001-9259-0359 1], *Mátyás Krisztián Baracza*[0000-0002-7809-9069 1*]

[1] Research Institute of Applied Earth Sciences, University of Miskolc, Hungary
https://doi.org/10.47833/2024.3.ENG.008

***Keywords:***
DBHE
Abandoned Oilfield Wells
Heat Production
Geothermal Energy
Numerical Analysis

***Article history:***
Received 31. October 2023
Revised 5. November 2024
Accepted 10. November 2024

***Abstract***
*Heat production from abandoned oilfield wells retrofitted into coaxial deep borehole heat exchangers (DBHEs) have become a hot topic in the past decade, since the utilization of geothermal energy drew increased attention due to the volatility of the energy prices. Numerous studies investigate performance enhancement possibilities of such systems, all agreeing that the circulation rate is one of the strongest driving factors which influences total thermal output and sustainability. While these wells have several stages of cemented casings in the wellbore, each having size limitations on the production string, the annular and string cross-sectional flow areas, thus velocities of the countercurrent fluid streams could greatly influence the total heat output of the selected arrangement. Moreover, with each setup, heat contact surface between the formation and the parallel fluid columns changes, furtherly influencing the performance. This paper introduces a numerical model, where the authors have investigated several well structures under various circulation rates to determine optimal flow rate under continuous operation.*

## 1. Introduction

Borehole heat exchangers, especially deep coaxial arrangements have increased in popularity in the past decades due to the fact that they can be easily retrofitted into existing deep wells. However, energy potential of those oilfield dry wells is limited to the geothermal heat available in the surrounding rock mass, an investigation should be done on each well in Hungary, as geothermal gradient and terrestrial heat flow is much above the world average, due to the favorable geological conditions of the Carpathian basin *[1]*.

While geological properties and the size of the cemented well casing cannot be changed, heat flow quality between the circulated working fluid columns and the well casing, thus the expected heat output can be fine-tuned via optimizing injection rate and the size of the production tubing *[3]*.

This paper presents a parametric study, where the authors have built numerical models, coupled with a Python automation interface in order investigate data gathered from various DBHE arrangements with different flow rates.

## 2. Model description

A reference model has been built in *FlexPDE*, a finite element software *[4]*. A great advantage of the selected software is its option to describe the whole system in a single script file, which was then fed into the solver to generate the requested output files.

* Contact author: Mátyás Krisztián Baracza E-mail: krisztian.baracza@uni-miskolc.hu

Model geometry was defined in cylindrical coordinates, which resulted in greatly reduced simulation times with the same accuracy. Dimensions and each thermodynamic property of the environment have been carefully selected. These variables are summarized in the table below:

***Table 1.:*** *DBHE mesh sub-geometry dimensions with their thermodynamic properties*

| *SUB GEOMETRY* | *R [m]* | *Z [m]* | *k [W/mK]* | *Cp [J/kgK]* | *Density [kg/m3]* |
|---|---|---|---|---|---|
| Lithology | 40 | 2050 | 1.79 | 960 | 2100 |
| Cement | 0.10-0.15 | 2000 | 1.70 | 1350 | 2000 |
| Casing | 0.06-0.11 | 2000 | 54 | 490 | 7850 |
| Tubing | 0.03-0.08 | 2000 | 54 | 490 | 7850 |
| Fluid (inner/outer) | VAR | 2000 | 0.6 | 4200 | 1000 |

Proportions of the annular and string cross-sections were also added as an input variable to calculate countercurrent fluid flow velocities at model mesh initialization:

***Table 2.:*** *Cross-sectional areas and their proportion for each casing/tubing combination*

| **ANNULAR & TOOLSTRING CROSS-SECTION [cm2]** | | | | | | | |
|---|---|---|---|---|---|---|---|
| | | **IR(tubing) [m]** | | | | | |
| | | **0,03** | **0,04** | **0,05** | **0,06** | **0,07** | **0,08** |
| **OR(casing) [m]** | **0,06** | 28,27 | N.A. | N.A. | N.A. | N.A. | N.A. |
| | **0,07** | 62,83 | 34,56 | N.A. | N.A. | N.A. | N.A. |
| | **0,08** | 103,67 | 75,40 | 40,84 | N.A. | N.A. | N.A. |
| | **0,09** | 150,79 | 122,52 | 87,96 | 47,12 | N.A. | N.A. |
| | **0,10** | 204,20 | 175,92 | 141,37 | 105,28 | 53,41 | N.A. |
| | **0,11** | 263,89 | 235,61 | 201,06 | 160,22 | 113,09 | 59,69 |
| **STRING AREA** | | 28,27 | 50,26 | 78,54 | 113,09 | 153,93 | 201,06 |

| **CROSS-SECTIONAL PROPORTION [-]** | | | | | | | |
|---|---|---|---|---|---|---|---|
| | | **IR(tubing) [m]** | | | | | |
| | | **0,03** | **0,04** | **0,05** | **0,06** | **0,07** | **0,08** |
| **OR(casing) [m]** | **0,06** | 1,000 | N.A. | N.A. | N.A. | N.A. | N.A. |
| | **0,07** | 2,222 | 0,688 | N.A. | N.A. | N.A. | N.A. |
| | **0,08** | 3,667 | 1,500 | 0,520 | N.A. | N.A. | N.A. |
| | **0,09** | 5,333 | 2,438 | 1,120 | 0,417 | N.A. | N.A. |
| | **0,10** | 7,222 | 3,500 | 1,800 | 0,889 | 0,347 | N.A. |
| | **0,11** | 9,333 | 4,688 | 2,560 | 1,417 | 0,735 | 0,297 |

Surface temperature was set to 12°C, with a linearly increasing vertical geothermal gradient of 0.042 °C/m. The resulting temperature gradient was added to the model boundary as a constant thermal recovery to the model. An additional 50 m buffer region was added to the bottom of the DBHE. Each model was run with a constant temperature injection on constant flow rate.

Velocity vectors, being proportional with the cross-sectional flow area of each flow profile, were calculated from the flow rate:

$$A_1(-v_o) + A_2 v_i = 0 \tag{1}$$

where $-v_o$ is the annular and $v_i$ is the string fluid velocity. For coaxial arrangements, having a static flow rate and uniform cross-section through the pipe gives countercurrent velocities from the following formulae:

$$v_i = \frac{Q}{3600} IR_{tbg}^2 \pi \left[\frac{m}{s}\right] \tag{2}$$

$$v_o = -v_i \frac{IR_{tbg}^2}{IR_{csg}^2 - OR_{tbg}^2} \tag{3}$$

where $IR_{csg}$ is the casing inner radius, $OR_{tbg}$ and $IR_{tbg}$ are tubing radii. For cylindrical models with reverse circulation, a good practice is to calculate the temperature average of the annular bottom cells and force that value to be the inlet temperature of the inner fluid column, which should be recorded for each timestep as bottom fluid temperature.

Model energy equation was derived from the following general heat equation:

$$\frac{\partial}{\partial x}\left(k\frac{\partial T}{\partial x}\right)+\frac{\partial}{\partial y}\left(k\frac{\partial T}{\partial y}\right)+\frac{\partial}{\partial z}\left(k\frac{\partial T}{\partial z}\right)+q=\rho Cp\frac{\partial T}{\partial t} \quad (4)$$

As the model do not have any internal heat source, $q$ was neglected. While, flowing fluid raises unstable temperature conditions (where $q \neq 0$) a convective coefficient was added to the right side of the formula:

$$\frac{\partial}{\partial x}\left(k\frac{\partial T}{\partial x}\right)+\frac{\partial}{\partial y}\left(k\frac{\partial T}{\partial y}\right)+\frac{\partial}{\partial z}\left(k\frac{\partial T}{\partial z}\right)=\rho C_p\frac{\partial T}{\partial t}+\rho_f Cp_f V_z\frac{\partial T}{\partial z} \quad (5)$$

Eq. (5) is valid under cartesian coordinates. For cylindrical models, eq. (6) was used:

$$\frac{1}{r}\frac{\partial}{\partial r}\left(kr\frac{\partial T}{\partial r}\right)+\frac{\partial}{\partial z}\left(k\frac{\partial T}{\partial z}\right)=\rho C_p\frac{\partial T}{\partial t}+\rho_f Cp_f V_z\frac{\partial T}{\partial z} \quad (6)$$

For even better simulation times, we introduced a vertical scaling factor $Z_{scale}$ in the equation, which was also added into the geometry builder:

$$\frac{1}{r}\frac{\partial}{\partial r}\left(\frac{kr\frac{\partial T}{\partial r}}{Z_{scale}}\right)+\frac{\partial}{\partial z}\left(k\frac{\partial T}{\partial z}Z_{scale}\right)=\rho C_p\frac{\partial T}{\partial t}+\rho_f Cp_f V_z\frac{\partial T}{\partial z} \quad (7)$$

However, selection of the scaling factor should be handled with increased care because it may significantly increase model error *[6]*. Simulations were carried out with scaling factor of 1/200.

## 3. Results: Heat performance

According to *Table 2*, a total of 21 well profiles were generated according to the given casing and tubing radii. The smallest tubing diameter (0.06 m, similar to the inside diameter of the 2-7/8" production tubing) is expected to produce the highest flowline temperature for each fixed casing size. However, the main driving factor, apart from the injection temperature is the circulation rate, therefore we ran all simulation series with 5, 7.5, 10, 12.5 and 15 m$^3$/h constant flow rate, for 7 day (604 800s). This resulted the output data of 125 simulations, wherefrom we extracted bottom-hole fluid temperatures and wellhead (flowline) temperatures in labeled output text files for each simulation timestep. These files were then fed into a Python script which sorted them into an xlsx worksheet for analysis.

Heat performance of each arrangement was calculated with the mass flow rate (m) and the specific heat capacity of the working fluid (Cp) with the temperature change (dT), calculated from the temperature difference between the feed and the outlet *[2]*:

$$Q = m * Cp_f * dT \quad (8)$$

| | | | FLOWLINE TEMPERATURE [°C] | | | | | | | | HEAT PERFORMANCE [kW] | | | | | |
|---|---|---|---|---|---|---|---|---|---|---|---|---|---|---|---|---|
| FLOW RATE = 5 m3/h | | | IR(tubing) [m] | | | | | | | | IR(tubing) [m] | | | | | |
| | | | 0,03 | 0,04 | 0,05 | 0,06 | 0,07 | 0,08 | | | 0,03 | 0,04 | 0,05 | 0,06 | 0,07 | 0,08 |
| | OR(casing) [m] | 0,06 | 27,25 | N.A. | N.A. | N.A. | N.A. | N.A. | | 0,06 | 88,95 | N.A. | N.A. | N.A. | N.A. | N.A. |
| | | 0,07 | 29,16 | 27,02 | N.A. | N.A. | N.A. | N.A. | | 0,07 | 100,12 | 87,63 | N.A. | N.A. | N.A. | N.A. |
| | | 0,08 | 30,78 | 28,81 | 26,89 | N.A. | N.A. | N.A. | | 0,08 | 109,56 | 98,04 | 86,87 | N.A. | N.A. | N.A. |
| | | 0,09 | 32,14 | 30,32 | 28,51 | 26,82 | N.A. | N.A. | | 0,09 | 117,51 | 106,89 | 96,33 | 86,44 | N.A. | N.A. |
| | | 0,10 | 33,28 | 31,66 | 29,91 | 28,23 | 26,76 | N.A. | | 0,10 | 124,15 | 114,67 | 104,45 | 94,67 | 86,10 | N.A. |
| | | 0,11 | 34,43 | 32,64 | 31,15 | 29,46 | 28,15 | 26,73 | | 0,11 | 130,83 | 120,40 | 111,73 | 101,83 | 94,20 | 85,95 |

***Figure 1.:*** *Calculated flowline temperature and heat performance for Q=5 m$^3$/h (timestep: 7d)*

When null-point temperature being equal with the injection temperature, the highest wellhead temperature was achieved with the 0.03/0.11 arrangement on the lowest, 5 $m^3$/h flow rate, while heat performance peaked on the highest flow rate with the same dimensions. However, peak performance with increased $T_{null}$ for each model is expected with lower circulation rates for each timestep.

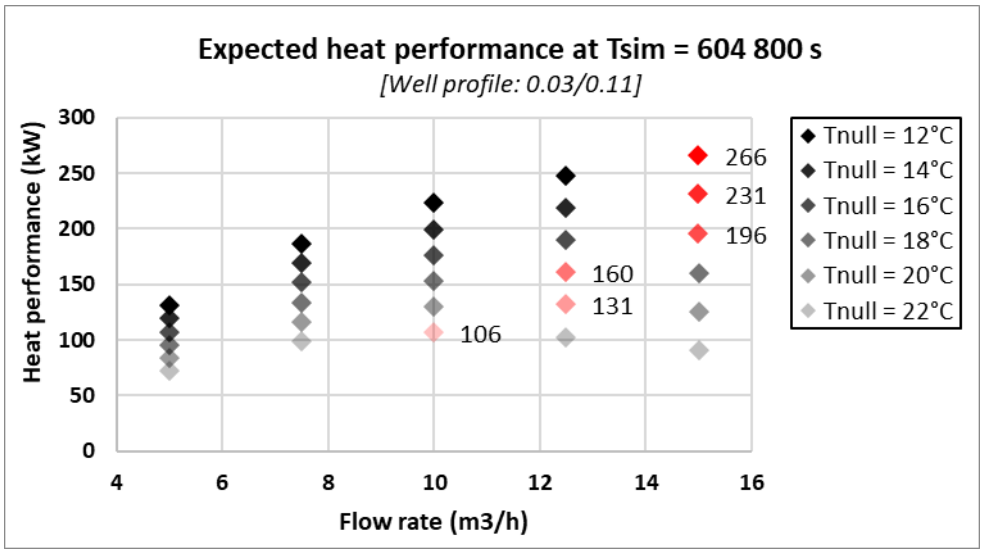


***Figure 2.:*** *Performance calculated from flowline temperature for each simulation. Maximum values, marked with red diamonds indicate that peak performance drops with reduced dT (valid for a specific timestep, under constant temperature injection).*

## 4. Results: Temperature profiles and thermal drawdown

We ran additional simulations to investigate temperature profiles of the working fluid. Profiles 0.03/0.11 and 0.03/0.06 were selected on 5 m3/h and simulation time was set to 1 year (31 536 000s). Additional surfaces were determined in every 100 m along the annular and the string region, where cell temperatures were averaged.

**FLUID TEMPERATURE PROFILE**

*[Q= 5 m3/h, Well profile: 0.03/0.11]*

| Depth [m] | t=1 d | | t=2 d | | t=5 d | | t=10 d | | t=20 d | | t=50 d | | t=100 d | | t=200 d | |
|---|---|---|---|---|---|---|---|---|---|---|---|---|---|---|---|---|
| | Str. | Ann. | Str. | Ann. | Str. | Ann. | Str. | Ann. | Str. | Ann. | Str. | Ann. | Str. | Ann. | Str. | Ann. |
| 0 | 38,1 | 12,0 | 36,7 | 12,0 | 34,9 | 12,0 | 33,9 | 12,0 | 32,9 | 12,0 | 31,7 | 12,0 | 31,0 | 12,0 | 30,2 | 12,0 |
| 100 | 43,0 | 16,0 | 41,2 | 15,8 | 39,2 | 15,5 | 37,9 | 15,3 | 36,7 | 15,1 | 35,4 | 15,0 | 34,5 | 14,8 | 33,6 | 14,7 |
| 200 | 45,7 | 19,3 | 43,8 | 18,8 | 41,6 | 18,3 | 40,2 | 17,9 | 38,9 | 17,6 | 37,5 | 17,3 | 36,5 | 17,1 | 35,5 | 16,9 |
| 300 | 48,3 | 22,5 | 46,2 | 21,8 | 43,9 | 21,0 | 42,4 | 20,6 | 41,0 | 20,1 | 39,4 | 19,6 | 38,3 | 19,3 | 37,3 | 19,0 |
| 400 | 50,7 | 25,8 | 48,6 | 24,9 | 46,0 | 23,9 | 44,5 | 23,2 | 42,9 | 22,7 | 41,3 | 22,0 | 40,1 | 21,6 | 39,0 | 21,2 |
| 500 | 53,1 | 29,1 | 50,8 | 28,0 | 48,2 | 26,7 | 46,5 | 26,0 | 44,9 | 25,2 | 43,1 | 24,5 | 41,9 | 23,9 | 40,7 | 23,4 |
| 600 | 55,4 | 32,4 | 53,0 | 31,1 | 50,2 | 29,6 | 48,5 | 28,7 | 46,8 | 27,9 | 44,9 | 26,9 | 43,6 | 26,3 | 42,4 | 25,7 |
| 700 | 57,7 | 35,7 | 55,2 | 34,3 | 52,2 | 32,6 | 50,4 | 31,5 | 48,6 | 30,5 | 46,7 | 29,4 | 45,3 | 28,7 | 44,0 | 28,0 |
| 800 | 59,8 | 39,1 | 57,2 | 37,4 | 54,2 | 35,5 | 52,2 | 34,3 | 50,4 | 33,2 | 48,3 | 32,0 | 46,9 | 31,1 | 45,6 | 30,4 |
| 900 | 61,9 | 42,4 | 59,2 | 40,5 | 56,0 | 38,5 | 54,0 | 37,1 | 52,1 | 35,9 | 50,0 | 34,5 | 48,5 | 33,6 | 47,1 | 32,7 |
| 1000 | 63,8 | 45,6 | 61,0 | 43,7 | 57,8 | 41,4 | 55,7 | 40,0 | 53,7 | 38,6 | 51,5 | 37,1 | 50,0 | 36,0 | 48,5 | 35,1 |
| 1100 | 65,6 | 48,9 | 62,8 | 46,8 | 59,5 | 44,3 | 57,3 | 42,8 | 55,3 | 41,3 | 53,0 | 39,6 | 51,4 | 38,5 | 49,9 | 37,4 |
| 1200 | 67,4 | 52,1 | 64,5 | 49,9 | 61,0 | 47,2 | 58,8 | 45,5 | 56,7 | 43,9 | 54,4 | 42,2 | 52,7 | 40,9 | 51,2 | 39,8 |
| 1300 | 68,9 | 55,3 | 66,0 | 52,9 | 62,5 | 50,1 | 60,2 | 48,3 | 58,1 | 46,6 | 55,7 | 44,7 | 54,0 | 43,3 | 52,4 | 42,1 |
| 1400 | 70,4 | 58,4 | 67,4 | 55,9 | 63,8 | 52,9 | 61,5 | 51,0 | 59,3 | 49,2 | 56,8 | 47,2 | 55,1 | 45,7 | 53,5 | 44,4 |
| 1500 | 71,7 | 61,5 | 68,7 | 58,9 | 65,0 | 55,7 | 62,7 | 53,7 | 60,4 | 51,8 | 57,9 | 49,6 | 56,2 | 48,1 | 54,5 | 46,7 |
| 1600 | 72,9 | 64,5 | 69,8 | 61,8 | 66,1 | 58,5 | 63,7 | 56,4 | 61,4 | 54,3 | 58,9 | 52,0 | 57,1 | 50,4 | 55,4 | 49,0 |
| 1700 | 73,9 | 67,5 | 70,8 | 64,6 | 67,1 | 61,2 | 64,7 | 58,9 | 62,3 | 56,8 | 59,7 | 54,4 | 57,9 | 52,7 | 56,2 | 51,2 |
| 1800 | 74,7 | 70,3 | 71,6 | 67,4 | 67,9 | 63,8 | 65,4 | 61,5 | 63,1 | 59,3 | 60,4 | 56,7 | 58,6 | 55,0 | 56,9 | 53,3 |
| 1900 | 75,4 | 73,2 | 72,3 | 70,1 | 68,5 | 66,4 | 66,0 | 64,0 | 63,7 | 61,6 | 61,0 | 59,0 | 59,2 | 57,2 | 57,4 | 55,5 |
| 2000 | 75,9 | 76,0 | 72,8 | 72,9 | 69,0 | 69,1 | 66,5 | 66,6 | 64,2 | 64,2 | 61,5 | 61,5 | 59,6 | 59,6 | 57,9 | 57,9 |

**FLUID TEMPERATURE PROFILE**

*[Q= 5 m3/h, Well profile: 0.03/0.06]*

| Depth [m] | t=1 d | | t=2 d | | t=5 d | | t=10 d | | t=20 d | | t=50 d | | t=100 d | | t=200 d | |
|---|---|---|---|---|---|---|---|---|---|---|---|---|---|---|---|---|
| | Str. | Ann. | Str. | Ann. | Str. | Ann. | Str. | Ann. | Str. | Ann. | Str. | Ann. | Str. | Ann. | Str. | Ann. |
| 0 | 28,8 | 12,0 | 28,2 | 12,0 | 27,5 | 12,0 | 27,0 | 12,0 | 26,6 | 12,0 | 26,0 | 12,0 | 25,6 | 12,0 | 25,2 | 12,0 |
| 100 | 32,4 | 15,8 | 31,7 | 15,7 | 30,8 | 15,5 | 30,2 | 15,4 | 29,7 | 15,3 | 29,0 | 15,1 | 28,5 | 15,0 | 28,0 | 15,0 |
| 200 | 35,7 | 19,3 | 34,9 | 19,0 | 33,8 | 18,7 | 33,1 | 18,5 | 32,5 | 18,2 | 31,7 | 18,0 | 31,1 | 17,8 | 30,6 | 17,7 |
| 300 | 38,9 | 22,8 | 38,0 | 22,4 | 36,8 | 21,9 | 36,0 | 21,6 | 35,3 | 21,3 | 34,4 | 20,9 | 33,7 | 20,6 | 33,1 | 20,4 |
| 400 | 42,0 | 26,3 | 41,0 | 25,8 | 39,7 | 25,1 | 38,8 | 24,7 | 38,0 | 24,3 | 37,0 | 23,8 | 36,3 | 23,5 | 35,6 | 23,1 |
| 500 | 45,1 | 29,8 | 44,0 | 29,2 | 42,6 | 28,4 | 41,6 | 27,9 | 40,7 | 27,4 | 39,6 | 26,8 | 38,8 | 26,3 | 38,1 | 25,9 |
| 600 | 48,2 | 33,4 | 47,0 | 32,6 | 45,4 | 31,7 | 44,4 | 31,0 | 43,4 | 30,4 | 42,2 | 29,7 | 41,3 | 29,2 | 40,5 | 28,7 |
| 700 | 51,1 | 36,9 | 49,8 | 36,0 | 48,1 | 34,9 | 47,0 | 34,2 | 45,9 | 33,5 | 44,7 | 32,6 | 43,7 | 32,1 | 42,9 | 31,5 |
| 800 | 54,0 | 40,3 | 52,6 | 39,4 | 50,8 | 38,1 | 49,6 | 37,3 | 48,4 | 36,5 | 47,1 | 35,6 | 46,1 | 34,9 | 45,2 | 34,3 |
| 900 | 56,7 | 43,8 | 55,3 | 42,7 | 53,3 | 41,3 | 52,1 | 40,4 | 50,9 | 39,5 | 49,4 | 38,5 | 48,3 | 37,7 | 47,4 | 37,0 |
| 1000 | 59,4 | 47,1 | 57,8 | 46,0 | 55,8 | 44,4 | 54,5 | 43,5 | 53,2 | 42,5 | 51,6 | 41,3 | 50,5 | 40,5 | 49,5 | 39,7 |
| 1100 | 61,9 | 50,5 | 60,3 | 49,2 | 58,1 | 47,5 | 56,7 | 46,5 | 55,4 | 45,4 | 53,7 | 44,1 | 52,6 | 43,2 | 51,5 | 42,4 |
| 1200 | 64,3 | 53,7 | 62,6 | 52,4 | 60,3 | 50,6 | 58,9 | 49,4 | 57,4 | 48,3 | 55,7 | 46,9 | 54,5 | 45,9 | 53,4 | 45,0 |
| 1300 | 66,5 | 56,9 | 64,7 | 55,4 | 62,3 | 53,5 | 60,9 | 52,3 | 59,4 | 51,1 | 57,6 | 49,6 | 56,3 | 48,5 | 55,1 | 47,5 |
| 1400 | 68,5 | 60,0 | 66,7 | 58,4 | 64,2 | 56,4 | 62,7 | 55,1 | 61,2 | 53,8 | 59,3 | 52,2 | 58,0 | 51,1 | 56,8 | 50,0 |
| 1500 | 70,4 | 63,0 | 68,5 | 61,4 | 65,9 | 59,2 | 64,4 | 57,8 | 62,8 | 56,4 | 60,9 | 54,7 | 59,5 | 53,5 | 58,3 | 52,4 |
| 1600 | 72,0 | 65,9 | 70,1 | 64,2 | 67,5 | 61,9 | 65,9 | 60,4 | 64,2 | 58,9 | 62,3 | 57,2 | 60,9 | 55,9 | 59,6 | 54,7 |
| 1700 | 73,5 | 68,7 | 71,5 | 66,9 | 68,8 | 64,4 | 67,2 | 62,9 | 65,5 | 61,3 | 63,5 | 59,5 | 62,1 | 58,1 | 60,7 | 56,9 |
| 1800 | 74,6 | 71,4 | 72,6 | 69,4 | 69,9 | 66,9 | 68,2 | 65,3 | 66,5 | 63,6 | 64,5 | 61,7 | 63,0 | 60,3 | 61,7 | 59,0 |
| 1900 | 75,5 | 73,9 | 73,5 | 71,8 | 70,7 | 69,2 | 69,0 | 67,5 | 67,3 | 65,8 | 65,2 | 63,7 | 63,8 | 62,3 | 62,4 | 60,9 |
| 2000 | 76,1 | 76,2 | 74,1 | 74,1 | 71,2 | 71,3 | 69,6 | 69,6 | 67,8 | 67,9 | 65,8 | 65,8 | 64,3 | 64,3 | 62,9 | 62,9 |

***Figure 3.:*** *Fluid temperature profiles in the annular and string region for different timesteps.*

At zero-time, temperature of both fluid columns was equal to the temperature of the rock mass in each region, followed by a sudden drop of wellhead temperature after fluid bottoms-up. A great difference was observed in bottom hole temperatures between the two arrangements near simulation end-time. On the one hand, fluid velocity proportion is 9.33 between the two models, meaning slower particles and increased contact surface thus better heat drainage from the formation

at 0.03/0.11 well. On the other hand, it means that temperature of the bottom region is expected to be lower, with further zone of influence. While there is no insulation in the production string, heat flux between the two fluid columns has an influence on the temperature distribution and heat output, but it is considerably less with the tubing strings having the same diameter *[5]*.

Zone of influence, or thermal drawdown has a great impact on sustainability while continuous circulation is performed *[7]*. Along with fluid profiles, we had run an additional simulation and recorded the temperature of additional 12 additional profiles in the formation cells from 0.2 to 40 m (252 points) on well profile 0.03/0.11, then evaluation and visualization of the text output files was done with a Python script.

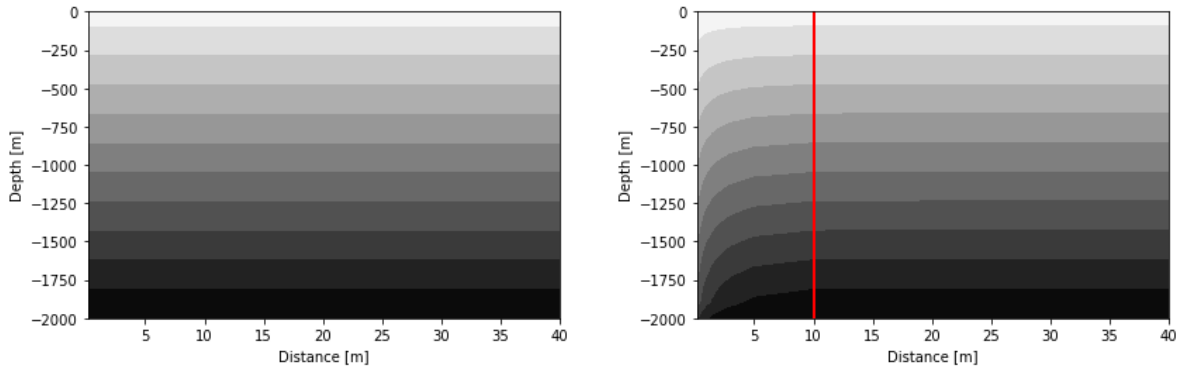


***Figure 4.:*** *Initial heat distribution in the model area [left] and heat distribution with indicating the zone of influence [right] after 185 d simulation time of the 0.03/0.11 (5 m3/h) model.*

Sensitivity of the temperature difference was set to 0.1°C to the zero-time reference thermal profile. As the red vertical line indicates, the zone of influence boundary at 10 m was reached after 185 days of simulation time, while the next monitored profile at 15 m was not reached until simulation end time with the selected flow rate. As linear interpolation, especially in closer regions of the wellbore should be avoided, development of interpolation algorithm is in progress, which will provide an exact determination of ZOI boundary at any time step.

## 5. Conclusion

We had successfully built a DBHE reference model in *FlexPDE* environment and had run multiple simulations with a set of casing/tubing diameters and several circulation rates. While with each circulation rate, best performance was achieved with the highest velocity difference between the string and annular flow, performance peak with reduced utilization (increased null-point temperature) was found at lower circulation rates for several simulations.

Temperature profile analysis of the countercurrent fluids on the extreme minimum/maximum performance models was done, where significant difference of bottom hole and wellhead temperatures were observed, which was influenced by fluid velocity, annular contact surface and the evolving thermal drawdown around the wellbore.

Zone of influence estimation and visualization from formation temperature data was done with Python, where we tested the script on 0.03/0.11 well profile, having the highest performance and the lowest bottom-hole temperature among the introduced well profiles. Zone of influence boundary for the selected simulation was between 10 and 15 m at the end of the 1-year simulation period.

For each model, even in optimized vertical scaling factor is a time-consuming task to run, analysis of additional simulation data is needed: this involves models with cyclic circulation, insulated well structures, or sustainability comparison of fixed performance (variable circulation rate) models.

## Acknowledgement

The research was carried out in the framework of the GINOP-2.3.2-15-2016- 00010 “Development of enhanced engineering methods with the aim at utilization of subterranean energy resources” project of the Research Institute of Applied Earth Sciences of the University of Miskolc in the framework of the Széchenyi 2020 Plan, funded by the European Union, co-financed by the European Structural and Investment Funds.

## References

[1] Aniko N. Toth, Peter Szucs, Jozsef Pap, Attila Nyikos, David K. Fenerty: Converting Abandoned Hungarian Oil and Gas wells into Geothermal Sources - PROCEEDINGS, 43rd Workshop on Geothermal Reservoir Engineering - Stanford University, Stanford, California, SGP-TR-213.

[2] C. Alimonti, D. Berardi, D. Bocchetti, E. Soldo: Coupling of energy conversion systems and wellbore heat exchanger in a depleted oil well - Geothermal Energy 4(1):11 DOI: 10.1186/s40517-016-0053-9

[3] C. Alimonti, E. Soldo, D. Bocchetti, D. Berardi: The wellbore heat exchangers: A technical review - Renewable Energy 123 (2018) 353-381. DOI: 10.1016/j.renene.2018.02.055

[4] PDE Solutions Inc. - FlexPDE 6: PDE Solutions Inc.; 2011.

[5] Richard A. Beier, José Acuña, Palne Mogensen, Björn Palm: Transient heat transfer in a coaxial borehole heat exchanger - Geothermics 51 (2014) 470-482. DOI: 10.1016/j.geothermics.2014.02.006

[6] Templeton, J.D., Ghoreishi-Madiseh, S.A., Hassani, J.D. and Al-Khawaja M.J.: Abandoned petroleum wells as sustainable sources of geothermal energy, Elseviere, Energy, Volume 70, 1 (2014), 366-373

[7] Wenke Zhang, Hongxing Yang, Lin Lu, Zhaohong Fang: The heat transfer analysis and optimal design on borehole ground heat exchangers - Energy Procedia 61 (2014) 385-388. DOI: 10.1016/j.egypro.2014.11.1131